SUPPORTING INFORMATION

Room Temperature Patterning of Nanoscale MoS_2 Under an Electron Beam

Mohammad S. M. Saifullah,[1*] Mohamed Asbahi,[1] Maryam Binti-Kamran Kiyani,[1] Sing Shy Liow,[1] Surani Bin Dolmanan,[1] Anna Marie Yong,[1] Esther A. H. Ong,[2] Asadullah Ibn Saifullah,[2,3] Hui Ru Tan,[1] Neeraj Dwivedi,[4] Tanmay Dutta,[5] Ramakrishnan Ganesan,[6] Suresh Valiyaveettil,[2*] Karen S. L. Chong,[1] Sudhiranjan Tripathy[1*]

[1] *Institute of Materials Research and Engineering, A*STAR (Agency for Science, Technology, and Research), 2 Fusionopolis Way, #08-03 Innovis, Singapore 138634, Republic of Singapore*

[2] *Department of Chemistry, National University of Singapore, 3 Science Drive 3, Singapore 117543, Republic of Singapore*

[3] *Department of Electrical and Electronic Engineering, Imperial College, South Kensington Campus, London SW7 2AZ, United Kingdom*

[4] *CSIR-Advanced Materials and Processes Research Institute, Habibganj Naka, Hoshangabad Road, Bhopal-462 026, Madhya Pradesh, India*

[5] *Department of Electrical and Computer Engineering, National University of Singapore, 21 Lower Kent Ridge Road, Singapore 117576, Republic of Singapore*

[6] *Department of Chemistry, Birla Institute of Technology & Science, Pilani – Hyderabad Campus, Jawahar Nagar, Kapra Mandal, Hyderabad-500 078, Telangana, India*

[*] Corresponding authors' email addresses: M.S.M.S: saifullahm@imre.a-star.edu.sg ; S.V.: chmsv@nus.edu.sg ; S.T.: tripathy-sudhiranjan@imre.a-star.edu.sg

1. NMR Data of Dialkylxanthogen Dilsulfides and Molybdenum Thiocubanes with Different Xanthate Moieties

Figures S1 to S4 show the ^{1}H NMR spectra of dialkylxanthogen disulfides used in this study. The chemical shift values corresponding to the different environments of protons are denoted in the figure captions. The number of ^{1}H NMR signals corresponding to the precursors diethylxanthogen disulfide (EX), dipropylxanthogen disulfide (PX), di-*iso*-propylxanthogen disulfide (IPX), and dibutylxanthogen disulfide (BX) were found to be 2, 3, 2, and 4, respectively. The number of signals, splitting patterns, and their intensities matched well with the chemical structures of pure dialkylxanthogen disulfides. After chelation with molybdenum, each signal in the thiocubanes (MoS_2-EX, MoS_2-PX, MoS_2-IPX, and MoS_2-BX) was found further splitting into two, while maintaining the spin multiplicity (Figure S5 to S8) corresponding to the parent alkyl groups. It is known from the literature that the alkylxanthates chelate in molybdenum thiocubane in two ways: terminal and bridging.[1] Out of the six xanthate ligands present in molybdenum thiocubanes, four are coordinated to the molybdenum ions in chelating bidendate fashion, while the remaining two are coordinated in bridging bidendate fashion. The established structures revealed that the ratio between terminal and bridging chelation is 2:1. Although in these studies the prepared thiocubanes were not purified by recrystallization (as they were deemed pure enough *via* the TGA studies for patterning, see §**2**), the two different chelating modes are clearly distinguished in ^{1}H NMR through the separation of characteristic protons in different chemical environments. For instance, in the case of non-chelated diethylxanthogen disulfide, the methylene and methyl protons appeared at 1.42, and 4.68 ppm as triplet and quartet, respectively. After chelation with Mo metal atom, each of these methylene and methyl protons in the obtained MoS_2-EX are further separated as two signals, while maintaining the spin multiplicity. Such a separation confirmed the chelation of ethylxanthate in terminal and bridging modes in a stoichiometry of ~2:1. This is true for other thiocubanes as well although there is a slight variation in this ratio due to the presence of minor impurities. However, these impurities do not affect the patterning studies.

NMR Data of Dialkylxanthogen Dilsulfides

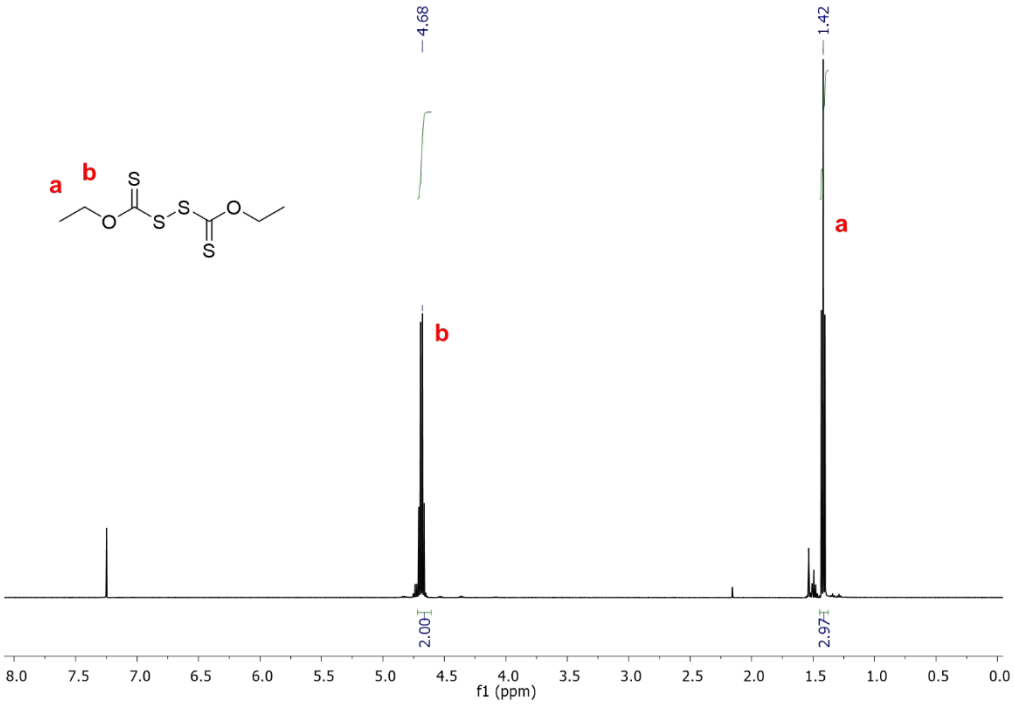

Figure S1: ^{1}H NMR spectrum of diethylxanthogen disulfide, in $CDCl_3$. ^{1}H NMR (δ [ppm], $CDCl_3$, 500 MHz, 24 °C): 1.42 (t, $OCH_2C\boldsymbol{H}_3$), 4.68 (q, $OC\boldsymbol{H}_2CH_3$).

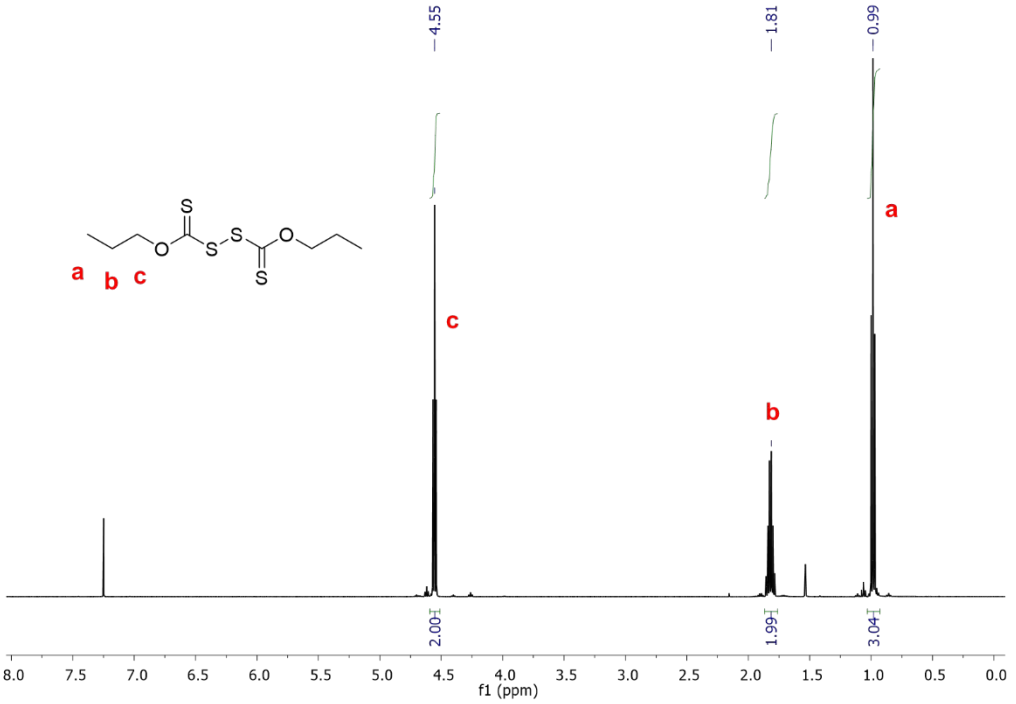

Figure S2: ^{1}H NMR spectrum of dipropylxanthogen disulfide, in $CDCl_3$. ^{1}H NMR (δ [ppm], $CDCl_3$, 500 MHz, 24 °C): 0.99 (t, $OCH_2CH_2C\boldsymbol{H}_3$), 1.81 (m, $OCH_2C\boldsymbol{H}_2CH_3$), 4.55 (t, $OC\boldsymbol{H}_2CH_2CH_3$).

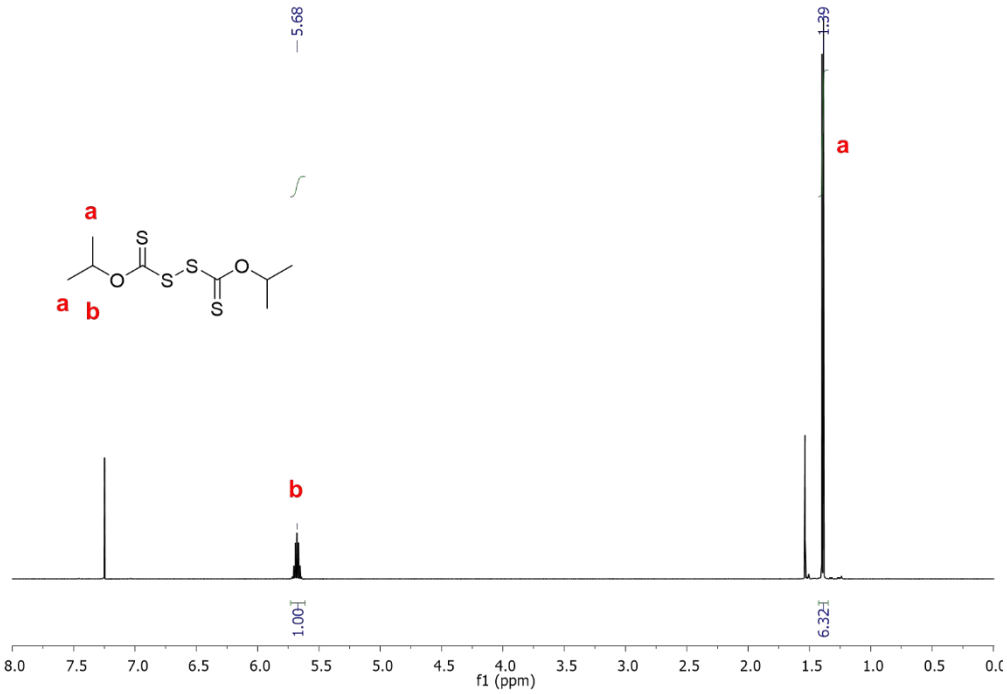

Figure S3: ^{1}H NMR spectrum of di-*iso*-propylxanthogen disulfide, in $CDCl_3$. ^{1}H NMR (δ [ppm], $CDCl_3$, 500 MHz, 24 °C): 1.39 (d, $OCH(C\boldsymbol{H}_3)_2$), 5.68 (m, $OC\boldsymbol{H}(CH_3)_2$).

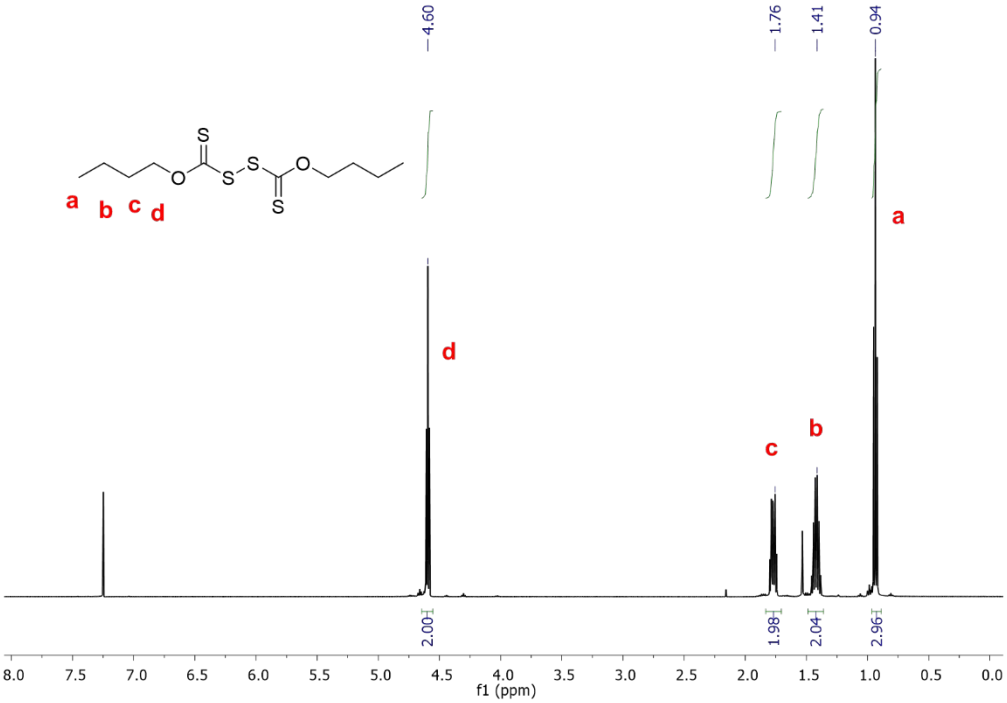

Figure S4: ^{1}H NMR spectrum of dibutylxanthogen disulfide, in $CDCl_3$. ^{1}H NMR (δ [ppm], $CDCl_3$, 500 MHz, 24 °C): 0.94 (t, $OCH_2CH_2CH_2C\boldsymbol{H}_3$), 1.41 (m, $OCH_2CH_2C\boldsymbol{H}_2CH_3$), 1.76 (m, $OCH_2C\boldsymbol{H}_2CH_2CH_3$), 4.60 (t, $OC\boldsymbol{H}_2CH_2CH_2CH_3$).

NMR Data of Molybdenum Thiocubanes with Different Xanthate Moieties

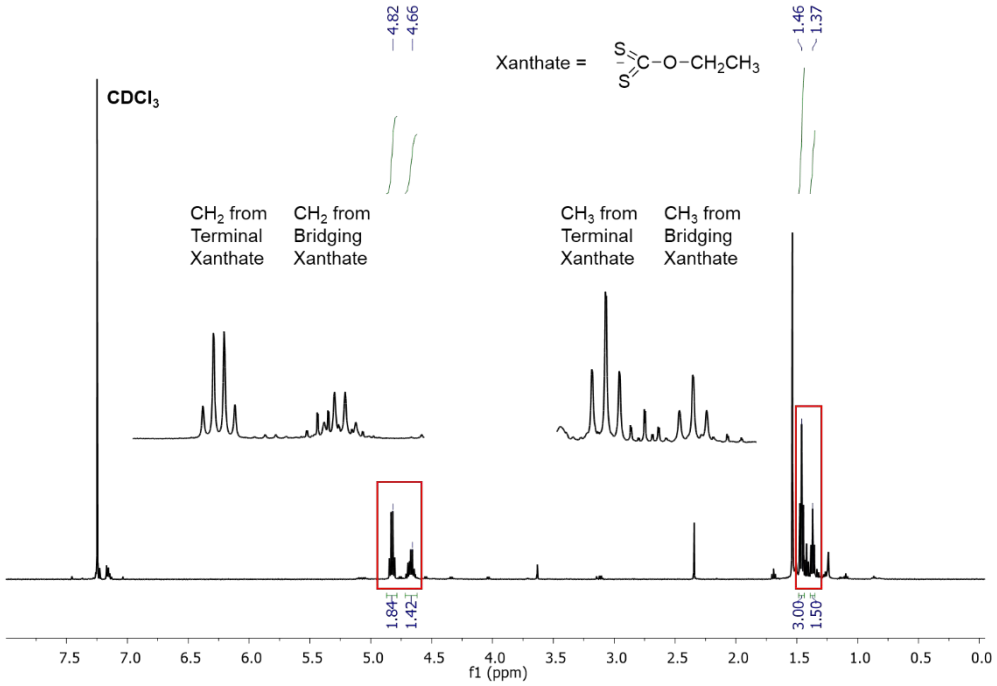

Figure S5: ^{1}H NMR spectrum of $Mo_4S_4(C_2H_5OS_2)_6$ (MoS_2-EX with ethyl xanthate moiety), in $CDCl_3$. ^{1}H NMR (δ [ppm], $CDCl_3$, 500 MHz, 24 °C): 1.37 – 1.46 (t, $OCH_2C\boldsymbol{H}_3$), 4.66 – 4.82 (q, $OC\boldsymbol{H}_2CH_3$).

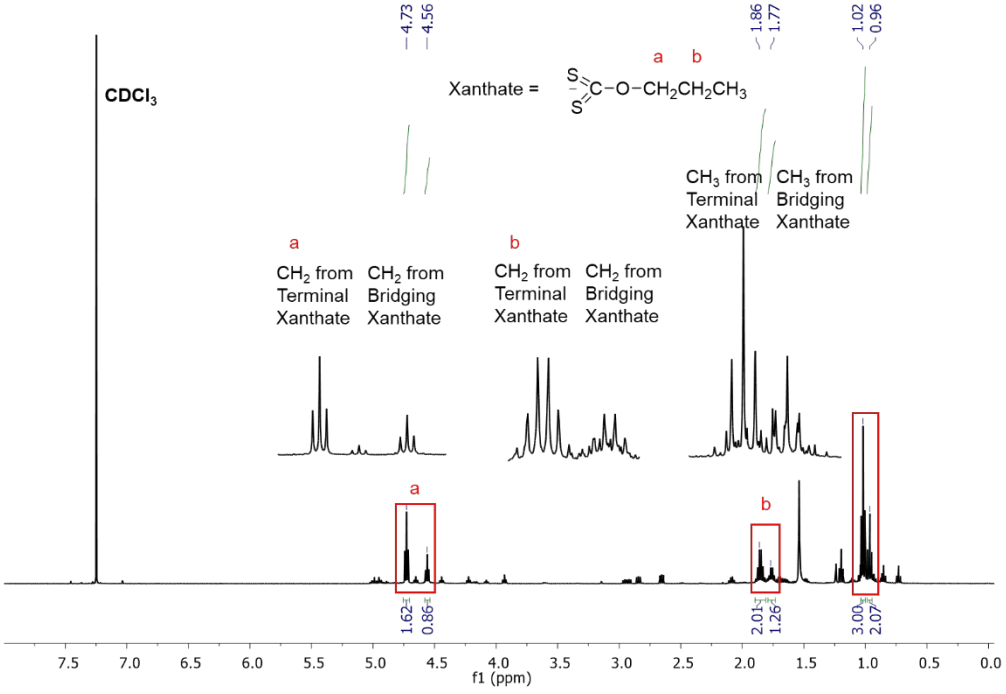

Figure S6: ^{1}H NMR spectrum of $Mo_4S_4(C_3H_7OS_2)_6$ (MoS_2-PX with propyl xanthate moiety), in $CDCl_3$. ^{1}H NMR (δ [ppm], $CDCl_3$, 500 MHz, 24 °C): 0.96 – 1.02 (t, $OCH_2CH_2C\boldsymbol{H}_3$), 1.77 – 1.86 (m, $OCH_2C\boldsymbol{H}_2CH_3$), 4.56 – 4.73 (t, $OC\boldsymbol{H}_2CH_2CH_3$).

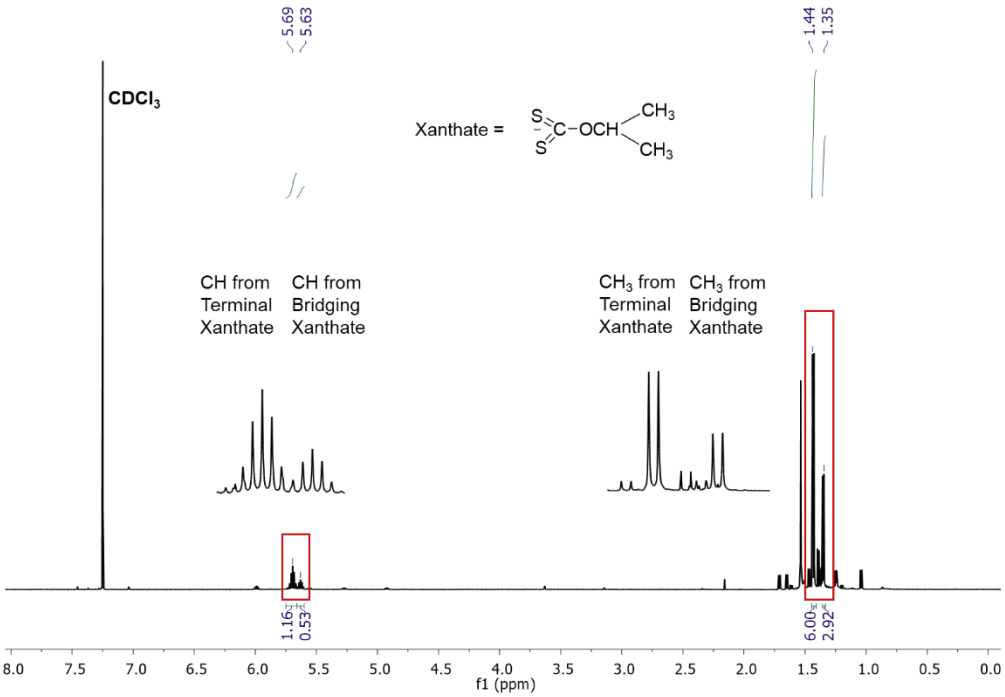

Figure S7: ^{1}H NMR spectrum of $Mo_4S_4(C_3{}^iH_7OS_2)_6$ (MoS_2-IPX with *iso*-propyl xanthate moiety), in $CDCl_3$. ^{1}H NMR (δ [ppm], $CDCl_3$, 500 MHz, 24 °C): 1.35 – 1.44 (t, $OCH(C\boldsymbol{H}_3)_2$), 5.63 – 5.69 (m, $OC\boldsymbol{H}(CH_3)_2$).

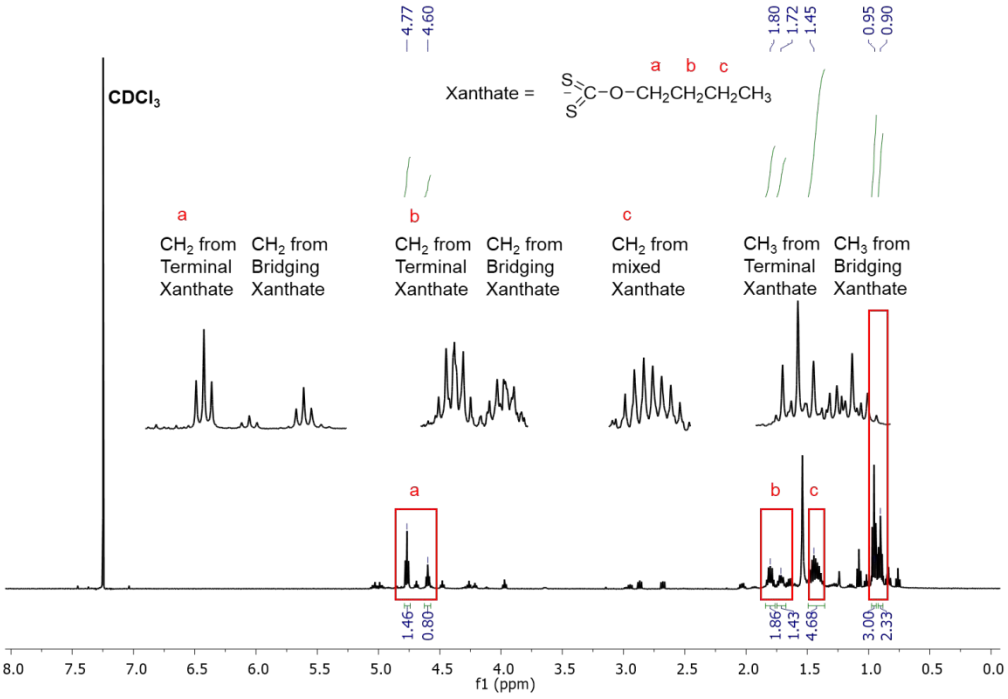

Figure S8: ^{1}H NMR spectrum of $Mo_4S_4(C_4H_9OS_2)_6$ (MoS_2-BX with butyl xanthate moiety), in $CDCl_3$. ^{1}H NMR (δ [ppm], $CDCl_3$, 500 MHz, 24 °C): 0.90 – 0.95 (t, $OCH_2CH_2CH_2C\boldsymbol{H}_3$), 1.45 (m, $OCH_2CH_2C\boldsymbol{H}_2CH_3$), 1.72 – 1.80 (m, $OCH_2C\boldsymbol{H}_2CH_2CH_3$), 4.60 – 4.77 (t, $OC\boldsymbol{H}_2CH_2CH_2CH_3$).

2. Thermogravimetric Analysis (TGA) and Differential Scanning Calorimetry (DSC) of Molybdenum Thiocubanes

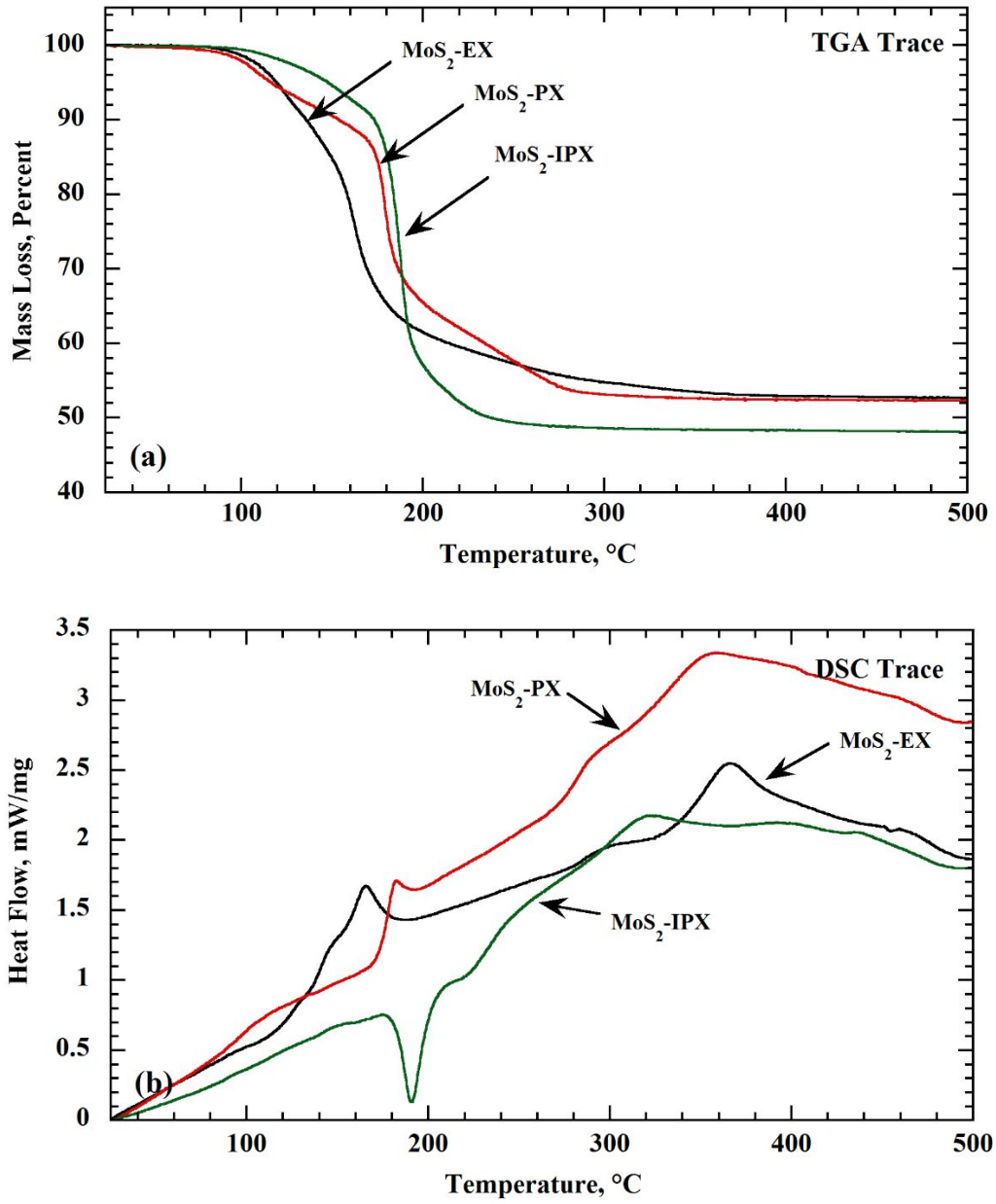

Figure S9: (a) TGA and (b) DSC of MoS_2–EX, MoS_2–PX, and MoS_2–IPX resists.

Table S1 below gives a comparison of percentage theoretical and experimental ceramic yields of MoS_2 for different molybdenum thiocubane resists at 500 °C as obtained from the TGA studies [Figure S9(a)]. It is interesting to note that the match between experimental and theoretical ceramic yields of MoS_2 for various thiocubane resists is very close. Minor discrepancy between them could be due to small amount of impurities present and/or incomplete decomposition at 500 °C.

Table S1: Comparison of percentage experimental and theoretical ceramic yields of MoS_2 for different molybdenum thiocubane resists at 500 °C.

Resist	Theoretical	Experimental
MoS_2–EX	51.7	52.7
MoS_2–PX	48.4	52.3
MoS_2–IPX	48.4	48.1
MoS_2–BX	45.9	49.6

Figure S9(b) shows DSC curves of various molybdenum thiocubanes resists. It is worthwhile noting that just like MoS_2–BX resist [Figure 3(b)], both MoS_2–EX and MoS_2–PX resists do not have a definite melting point and undergo solid-state decomposition with a minor exotherm at 166 and 183 °C, respectively. On the other hand, MoS_2–IPX resist appears to have a distinct melting point at 190 °C and concurrently also undergoes decomposition yielding MoS_2 as the final product. Interestingly, MoS_2–IPX resist shows a sharp mass loss unlike the other counterparts [Figure S9(a) and Figure 3(a)].

3. XPS Study of Heat-Treated MoS_2 Films Obtained from MoS_2-BX

X-ray photoelectron spectroscopy (XPS) is the key tool to characterize metal chalcogenides, specially the stoichiometry or phases of MoS_x layers based on the binding energy of Mo and S peaks and area ratio of Mo and S peaks.[2,3] Therefore, we carried out XPS measurements on ThermoFisher Scientific Theta Probe XPS using Al K_α radiation with an energy of 1486.7 eV as the x-ray source to further understand the effect of isothermal heat treatment on MoS_2-BX resist and then unveil phases of MoS_x. We also prepared an additional sample, namely, Mo metal, which is metallic Mo layer on Si substrate, to visualize how molybdenum's binding energy in MoS_2-BX resist samples shifts with respect to metallic Mo. A ~40 nm thick Mo layer was deposited by magnetron sputtering (AJA Inc.) in a class 10k cleanroom at base and working pressures of 1×10^{-9} Torr and 2×10^{-3} Torr, respectively, at Ar flow rate of 20 sccm with 60 W Watt DC power applied to the target. Since the samples were exposed to air before XPS measurements, the contaminant oxides and adventitious carbon are expected to be present on the samples surfaces. Therefore, the XPS spectra are recorded on the samples before sputter ("BS") cleaning and after sputter ("AS") cleaning. Figure S10(a) shows Mo 3d and S 2s spectra, and Figure S10(b) depicts S 2p spectra of various MoS_2-BX resist samples which underwent

different isothermal heat treatment from 250 °C to 500 °C. The metallic Mo before sputter cleaning [Mo metal BS in Figure S10(a)] displays characteristic Mo $3d_{5/2}$ and Mo $3d_{3/2}$ peaks at ~228.2 eV and 231.4 eV, respectively, resulting in Mo $3d_{5/2}$-$3d_{3/2}$ splitting of 3.2 eV which is consistent with the standard literature of metallic Mo.[4] However, Mo metal sample before sputter cleaning also shows two additional peaks located at 232.8 eV and 235.9 eV which correspond to molybdenum oxide (MoO_x) $3d_{5/2}$ and (MoO_x) $3d_{3/2}$, respectively,[4] thus confirming formation of surface oxides of Mo as contaminants. To overcome this concern, the Mo 3d spectrum was recorded after sputter cleaning [Mo metal AS in Figure S10(a)] which exhibits only two well defined peaks of metallic Mo namely Mo $3d_{5/2}$ and Mo $3d_{3/2}$, though slightly downshift in their peak positions are observed with respect to Mo 3d spectrum of Mo metal recorded before sputter cleaning.

Next, S 2s and Mo 3d spectra of all MoS_2-BX samples before sputter cleaning show four different peaks namely P_1, P_2, P_3 and P_4. In all the samples before sputter cleaning, the peak P_1 is observed at around 226.4-226.7 and peak P_2 is observed at around 229.3-229.5 eV which correspond to S 2s and Mo $3d_{5/2}$ peaks, respectively, of MoS_2.[2,3,5] Thus, these results clearly reveal accurate shift of Mo $3d_{5/2}$ peak in all heat-treated MoS_2-BX samples with respect to Mo metal sample, signifying the importance of preparing additional metallic Mo sample. However, as observed for Mo metal sample, all the heat-treated MoS_2-BX samples before sputter cleaning also indicate presence of MoO_x. The peak positions of $3d_{3/2}$ peak of MoS_2 and $3d_{5/2}$ peak of MoO_x are quite close to each other.[2] Therefore, peak P_2 in all MoS_2-BX samples before sputter cleaning [Figure S10(a)] could also have a some contribution from $3d_{5/2}$ peak of MoO_x.[2,3,5] On the other hand, peak P_4 corresponds to $3d_{3/2}$ peak of MoO_x.[2] Similarly, S 2p spectra [Figure S10(b)] of all MoS_2-BX samples before sputter cleaning reveal two peaks P_1 and P_2 which correspond to S $2p_{3/2}$ and S $2p_{1/2}$ of MoS_2.[3,5] Furthermore, XPS spectra are also recorded after sputter cleaning to remove the effect of surface oxygen contaminant. The Mo 3d spectra [Figure S10(a)] after sputtering cleaning for all the heat-treated MoS_2-BX clearly reveal only two well defined peaks $3d_{5/2}$ and $3d_{3/2}$ of MoS_2, though sputter induced down shift of these peaks are observed as indicated by the dashed line. This could be due to the sputter cleaning induced creation of defects and vacancies, thus causing down shift of $3d_{5/2}$ and $3d_{3/2}$ peaks of MoS_2.[5] The sputter induced structural alteration is also visualized in sulfur element as the S 2s peak [Figure S10(b)] experienced downshift, S $2p_{3/2}$ and $2p_{1/2}$ peaks encountered down shift, and $2p_{1/2}$ peak weaken with respect to their XPS spectra recorded before sputter cleaning.

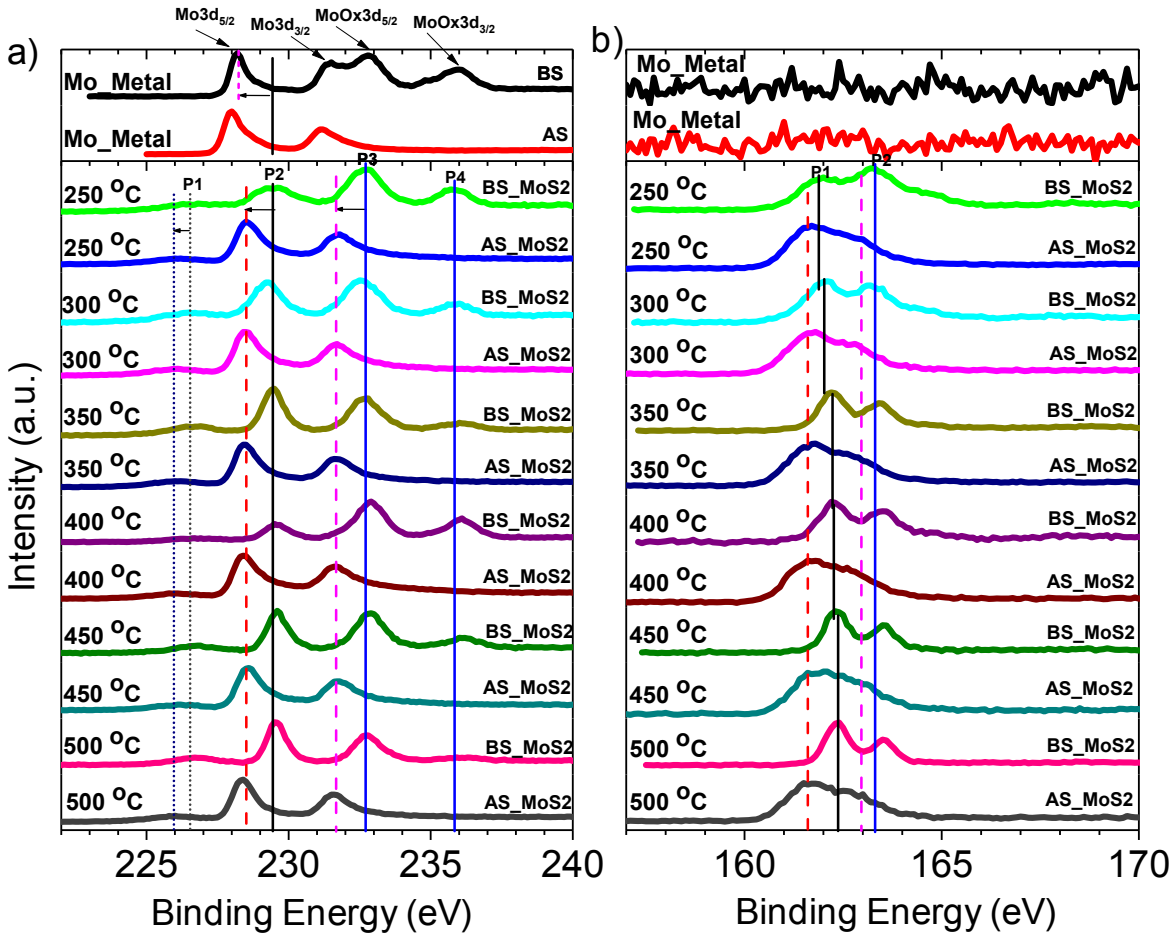

Figure S10: (a) S 2s and Mo 3d spectra of all MoS_2-BX samples and additional Mo metal sample. (b) S 2p spectra of all MoS_2-BX samples and additional Mo metal sample. The spectra are recorded before sputter cleaning, as shown by BS, and after sputter cleaning as indicated by AS. The arrows in figure (a) and (b) indicate the possible down shift of the peaks. The S 2p and S 2s spectra do not show any S peak in Mo metal sample.

4. Estimation of S/Mo Ratio from the XPS Data

Next, the deconvolution of Mo 3d and S 2p XPS spectra was performed to estimate the Mo and S composition and hence stoichiometry of MoS_x of samples prepared at different isothermal heat treatment temperatures from 250-500 °C. The deconvolution was performed using the mixed Gaussian-Lorentzian component with background subtracted in Shirley mode. As an example, Figure S11 shows deconvoluted Mo 3d and S 2p spectra of sample prepared at heat treatment temperature of 500 °C. Mo 3d spectra revealed two well-defined peaks A and B which correspond to Mo $3d_{5/2}$ and Mo $3d_{3/2}$, respectively. Likewise, S 2p spectra showed two peaks namely A and B which are attributed to S $2p_{3/2}$ and S $2p_{1/2}$, respectively. An area ratio method was used, where the area of Mo 3d peaks and S 2p peaks, and their relative sensitivity

factors were taken into account, to estimate the S/Mo ratio of MoS_2-BX samples and hence stoichiometry of MoS_x. Results revealed the stoichiometry of these samples are given in Table S2.

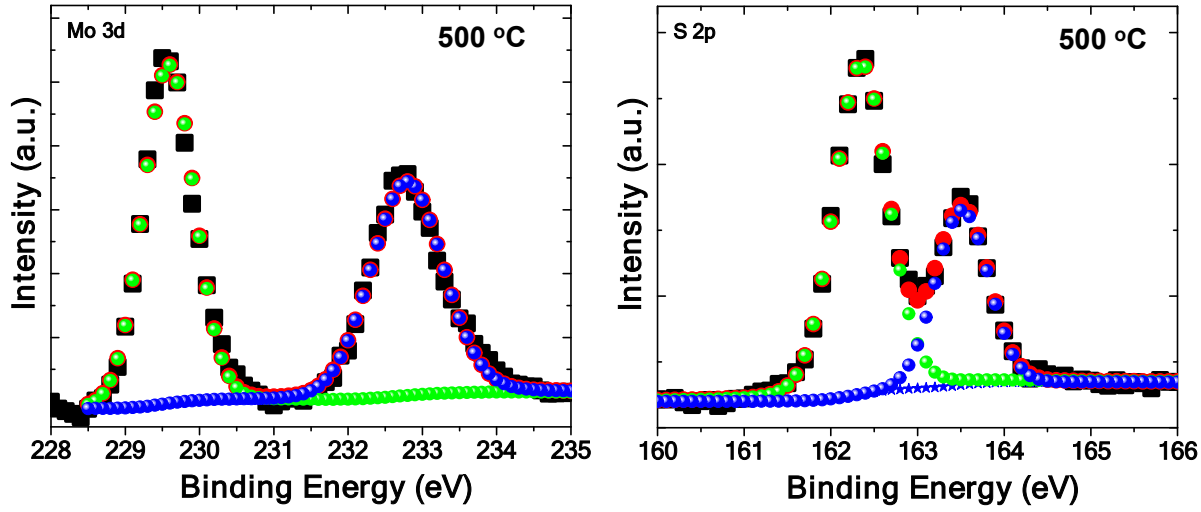

(a) (b)

Figure S11: Deconvolution of (a) Mo 3d and (b) S 2p spectra for the sample treated at 500 °C. The spectra were recorded on as-received sample without performing any sputtering on the sample.

Table S2: S/Mo ratios of samples obtained from the analysis of XPS data as described above.

Heat Treatment Temperature	S/Mo Ratio
250 °C	2.95
300 °C	2.79
350 °C	2.32
450 °C	1.7
500 °C	1.99

Molybdenum thiocubanes prepared in this work are sulfur-rich compounds with a S/Mo ratio of 4. MoS_2-BX, the thiocubane used to pattern MoS_2 starts to thermally decompose around 100 °C and reaches a stable mass at ~350 °C [Figure 3(a)]. This is also reflected in the XPS study where the S/Mo ratio steadily decreases with increasing isothermal heat-treatment temperature and stabilizes to a value of 2 at 500 °C. The S/Mo ratio of 1.7 at 450 °C appears to be an aberration.

5. Photoluminescence Spectra of Heat-Treated and Electron Beam Patterned MoS_2-BX

Room temperature micro-photoluminescence experiments were carried out on the samples using 488 nm Ar ion laser line excitation. The photoluminescence spectra from samples

isothermally heat-treated at different temperatures and exposed at various electron beam doses were recorded. As MoS_2 structures only show strong photoluminescence when they are in monolayer (or a few layers) form,[6] it is expected that the heat-treated and electron beam exposed patterned resist structures that are poorly crystalline would not show photoluminescence. Figure S12 shows very broad luminescence background signal around 550–750 nm range and multi-phonon Raman bands from $MoS_2/SiO_2/Si$ close to excitation line from heat-treated samples. There is no significant change in the line shape of the broad background to judge trend associated with temperature changes. However, the Raman signal observed from MoS_2 is enhanced with temperature treatment.

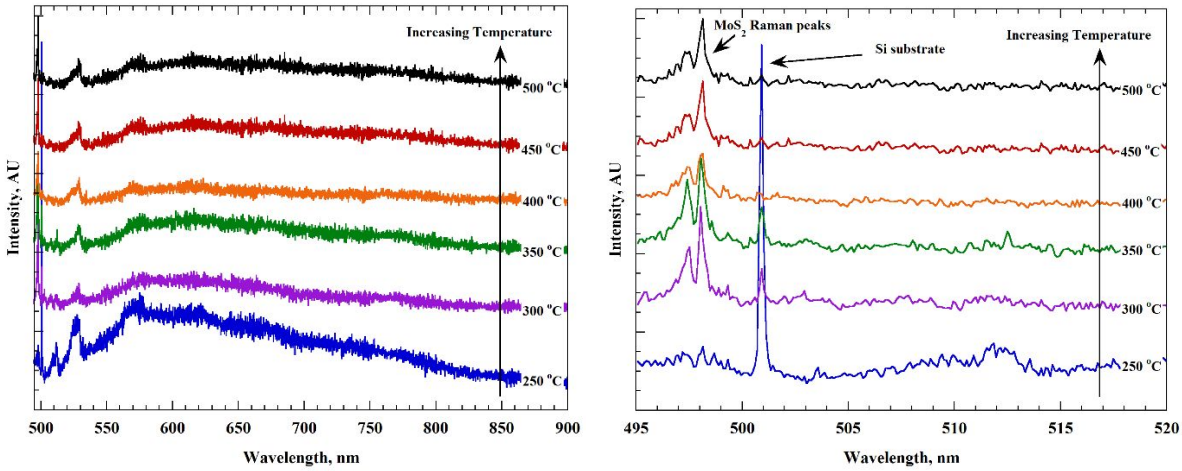

Figure S12: (left) Photoluminescence spectrum of MoS_2 films heat-treated at various temperatures. (Right) The zoomed in view showing the enhancement of Raman signal of MoS_2 with increasing heat-treatment temperature.

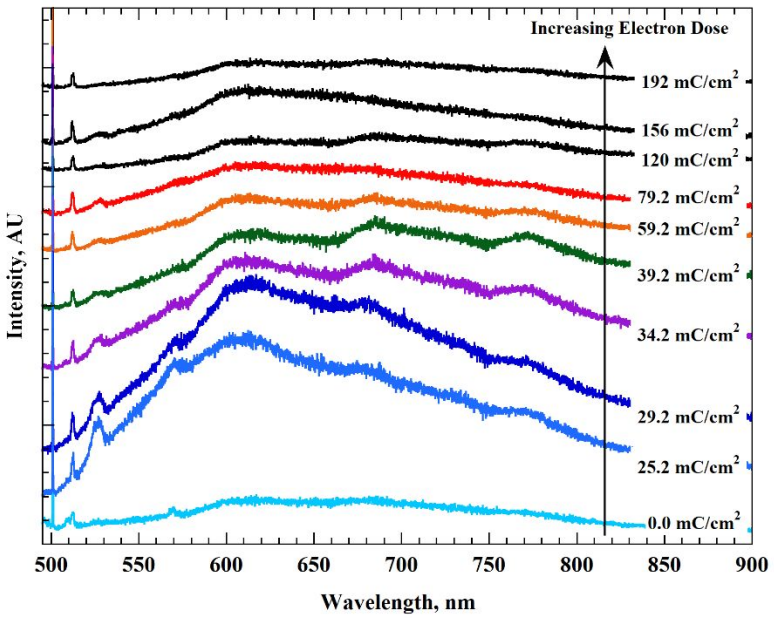

Figure S13: Photoluminescence spectrum of electron beam patterned MoS_2 discs exposed at different doses.

As seen from HR-TEM studies, there are MoS_2 flakes embedded within amorphous matrix in our patterns. This may not lead to significant band mixing effects to enhance the photoluminescence from MoS_2 which is seen from 2-D material. Figure S13 shows photoluminescence spectra of patterned samples obtained at different electron doses. The broad luminescence background around 550–750 nm does not show significant changes with electron doses. These observations clarify that the patterned structures are not luminescent MoS_2 while Raman experiments clearly show the formation of crystalline MoS_2 within the composite matrix.

6. Aspect Ratio of Patterned MoS_2-BX Lines

Approximately 10 nm wide lines of MoS_2-BX resist were patterned at various doses to gather accurately information about their aspect ratios. Using SEM imaging it was found that lines with lower doses not supported by a grid collapsed and showed the height of ~10 nm wide lines. The aspect ratio calculated was found to be slightly greater than 12 (Figure S14). Notice that the measured resist thickness is 125 nm.

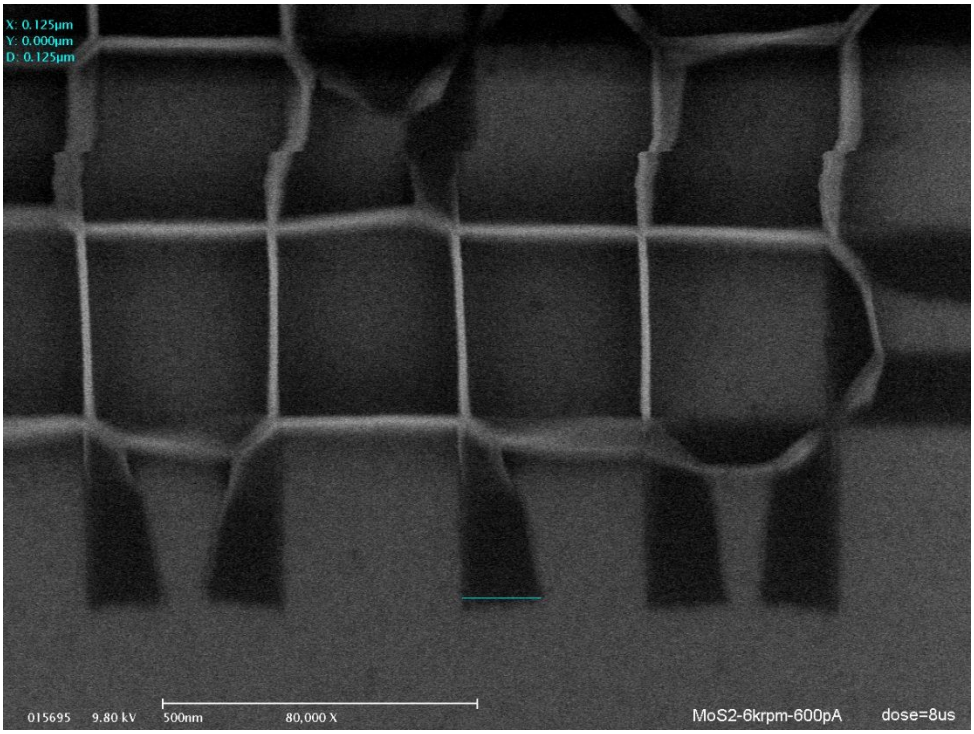

Figure S14: Aspect ratio of ~10 nm wide MoS_2-BX lines calculated using the collapsed structures.

7. Monte Carlo Simulation of 100 kV Electron Beam Passing Through a Resist on Silicon

Figure S15 shows Monte Carlo simulation of 100 kV electron beam passing through a resist coated on top of a silicon wafer.[7] The thickness of the resist is 125 nm and is assumed to be a molybdenum film that is deposited on silicon. It is worthwhile noticing that on and near the resist surface, there is very little loss of energy of the electron beam and also the lateral spread of the beam is small. However, a few microns below the surface, the electrons quickly start to lose energy and eventually come to rest due to scattering events.

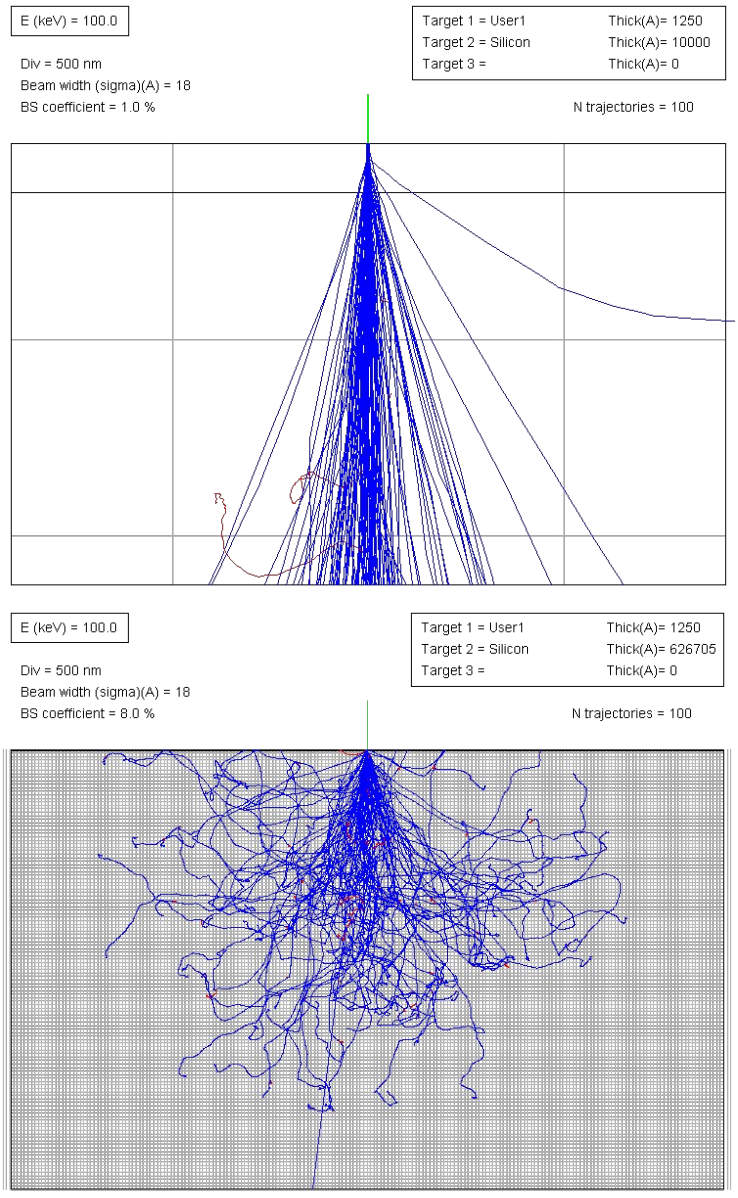

Figure S15: (Top) Monte Carlo simulation of 100 kV electron beam passing through 125 nm thick molybdenum sheet on top of 1 μm thick silicon showing very small beam spread in the resist. Horizontal line below the top surface is molybdenum-silicon interface. (Bottom) Monte Carlo simulation when 125 nm thick molybdenum sheet is on top of bulk silicon showing loss of energy over tens of microns and also lateral spread by nearly as much in the substrate.

8. Contrast Difference Between Bare Silicon Nitride Membrane and Patterned MoS_2 on Top

The set of figures below show the contrast difference between an amorphous silicon nitride membrane (left) and MoS_2 patterned on it (right). In the case of latter, the flakes of MoS_2 are clearly visible.

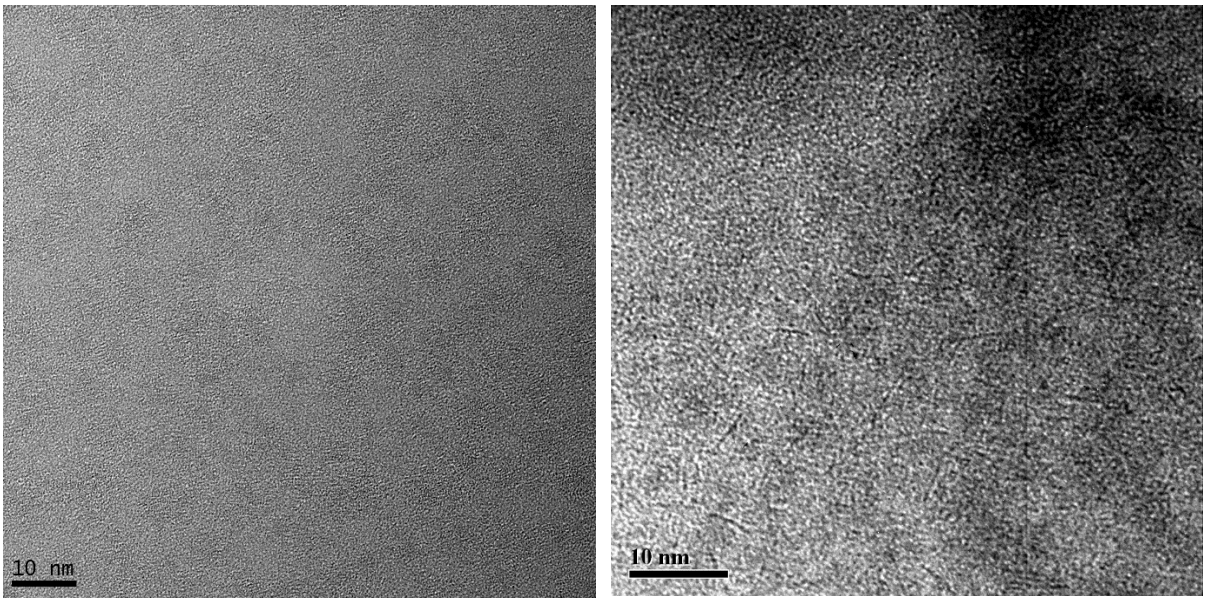

Figure S16: (Left) Contrast from a 30 nm thick amorphous silicon nitride membrane. (Right) Contrast from MoS_2 patterned at an electron dose of 34.2 mC/cm^2 on the same membrane. Notice the presence of MoS_2 flakes of various sizes.

9. AFM Images Showing Topography of Heat-Treated Molybdenum Thiocubane Films

Topography of molybdenum thiocubane resist heat-treated at various temperatures was examined using an AFM in tapping mode. Although the as-spin-coated films are air-stable and very smooth, leaving them in air for long periods of time (>3 weeks) lead to their slow chemical degradation with the films cracking and peeling off the surface [Figure S17]. The degradation also affects solubility of the films in organic solvents. Post-synthesis, it is best to store molybdenum thiocubanes in a fridge to prolong their shelf-life and use them when doing experiments.

Figure S18 shows the topography of heat-treated molybdenum thiocubane films (MoS_2-BX). It was observed that the films show higher topographical roughness at lower heat-treatment temperature (Average roughness R_{av} = 36.8 nm, 30.9 nm, 51.6 nm, 17.3, and 22.6 nm at 250 °C, 300 °C, 350 °C, 400 °C, and 450 °C, respectively). However, higher heat-treatment

temperature reduces the roughness with the best quality films obtained at 500 °C (R_{av} = 5.0 nm). Due to this reason, ellipsometry was used as the method of choice for measuring thickness of the films.

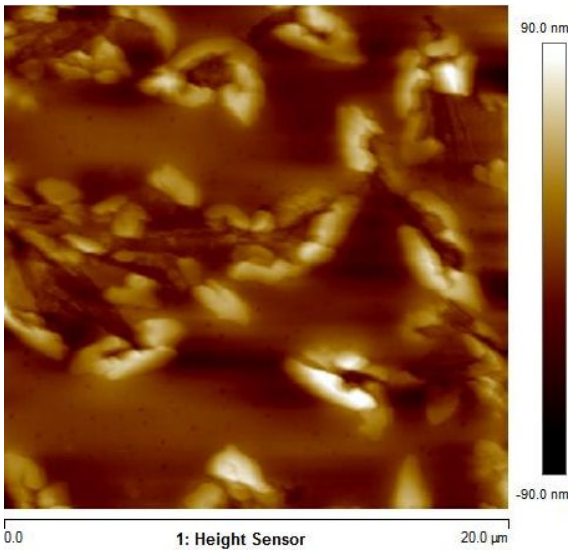

Figure S17: AFM topography of molybdenum thiocubane resist when left in air for >3 weeks.

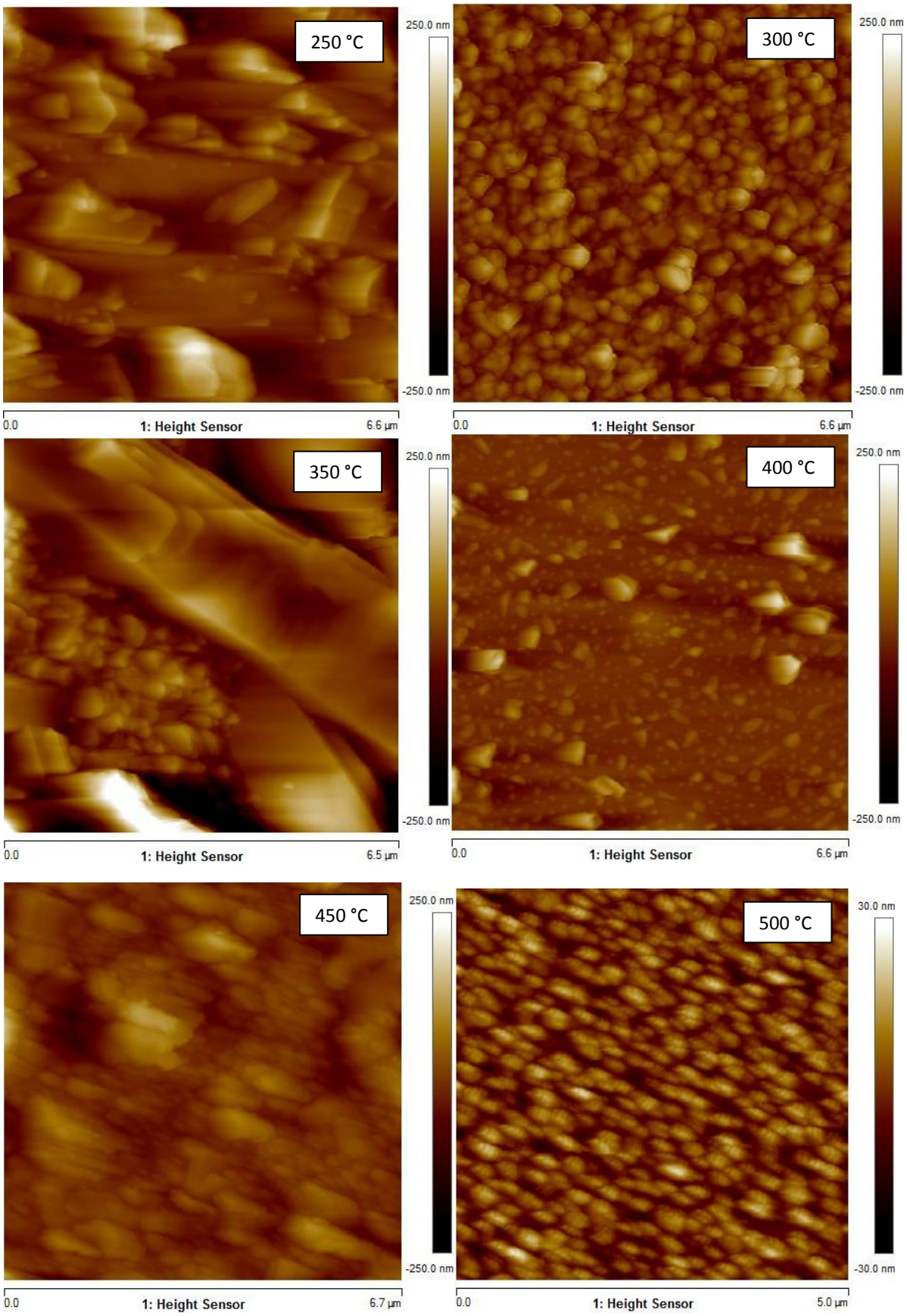

Figure S18: Topography of heat-treated molybdenum thiocubane films at various heat-treatment temperatures.

10. Thickness Variation as a Function of Electron Dose of MoS_2-BX Resist Used for micro-Raman Studies

For Raman spectroscopy studies, 50 μm diameter patterned discs of MoS_2-BX resist (~2 μm thick) were exposed at different electron doses. After exposure to electrons, the resist was developed in chloroform and rinsed in *iso*-propanol. This experiment is very similar to the electron beam sensitivity curves except that in the latter case a much thinner (~125 nm) resist was used (Figure 2). Although the electron beam sensitivity curves are shown to be "smooth" (Figure 2), in reality, the developed patterns show thickness variations which do not fall along the "smooth" curve. Only at fairly high electron doses, the thickness variation in the patterned resist somewhat "stabilizes". The cause of arbitrary thickness variations with dose is unclear, but it is believed to be a combination of stochastic nature of electron beam exposure of resist, post-exposure treatment of exposed areas in a developer, and rinsing. Thicker resists and strong developers make arbitrary thickness variations far worse. Inorganic resists show this property more than the organic ones as the former need stronger developers to completely remove unexposed resist film from substrate surface.[8,9] In this process, the exposed areas also get affected due to the lower contrast of resist, and hence their finite solubility in a strong developer in a range of intermediate doses, thus leading to arbitrary variations in thickness of the exposed resist. Figure S19 shows the normalized thickness variation with respect to dose for MoS_2-BX resist (~2 μm thick) used for micro-Raman studies. MoS_2-BX resist was developed in chloroform, a strong developer. Using a less strong developer such as acetone leaves a residue of MoS_2-BX resist on the silicon surface which is undesirable.

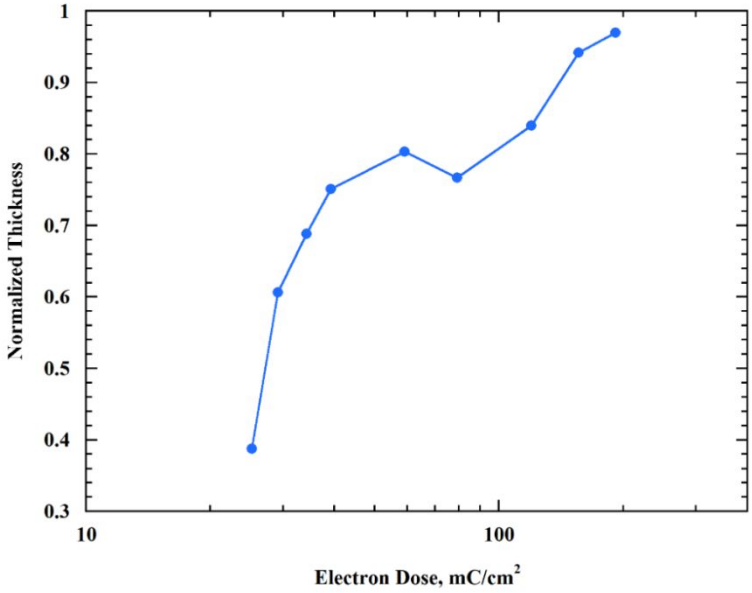

Figure S19: Change in the pattern thickness plotted with respect to electron dose for MoS_2-BX resist (~2 μm thick) used for micro-Raman studies.

Understandably, the effect of thickness variation is also felt in the characterization of exposed resist areas using Raman spectroscopy. Any reduction in patterned film thickness would lead to lower intensity of Raman peaks even though the electron dose may be higher [Figure 5(a)].

Comparing Figure S19 and Figure 5(a), it is clear that there is a variation of normalized thickness of patterns between 34.2 mC/cm^2 and 120 mC/cm^2 which is also reflected in the diminished intensity of Raman peaks even though the electron dose is higher.

References

1. Coyle, C. L.; Eriksen, K. A.; Farina, S.; Francis, J.; Gea, Y.; Greaney, M. A.; Guzi, P. J.; Halbert, T. R.; Murray, H. H.; Stiefel, E. I. Synthesis and Reactivity of Molybdenum-Sulfur Cubes. *Inorg. Chim. Acta*, **1992**, *198-200*, 565-575.

2. Liu, K-K.; Zhang, W.; Lee, Y-H.; Lin, Y-C.; Chang, M-T.; Su, C-Y.; Chang, C-S.; Li, H.; Shi, Y.; Zhang, H.; Lai, C-S.; Li, L-J. Growth of Large-Area and Highly Crystalline MoS_2 Thin Layers on Insulating Substrates. *Nano Lett*. **2012**, *12*, 1538-1544.

3. Baker, M. A.; Gilmore, R.; Lenardi, C.; Gissler, W. XPS Investigation of Preferential Sputtering of S From MoS_2 and Determination of MoS_x Stoichiometry From Mo and S Peak Position. *Appl. Surface Sci.* **1999**, 150, 255-262.

4. *NIST X-ray Photoelectron Spectroscopy Database*; NIST Standard Reference Database 20, Version 4.1. https://srdata.nist.gov/xps/ (accessed on 30th May 2019).

5. Chen, Y.; Huang, S.; Ji, X.; Adepalli, K.; Yin, K.; Ling, X.; Wang, X.; Xue, J.; Dresselhaus, M.; Kong, J.; Yildiz, B. Tuning Electronic Structure of Single Layer MoS_2 through Defect and Interface Engineering. *ACS Nano* **2018**, *12*, 2569-2579.

6. Eda, G.; Yamaguchi, H.; Voiry, D.; Fujita, T.; Chen, M.; Chhowalla, M. Photoluminescence from Chemically Exfoliated MoS_2. *Nano Lett.* **2011**, *11*, 5111-5116.

7. *EISS - Electron Beam Monte Carlo Simulator*. http://nanonems.imb-cnm.csic.es/index.php?option=com_content&view=article&id=25%3Aeiss-electron-beam-monte-carlo-simulator&catid=2%3Ananofabrication&Itemid=9&lang=en (accessed on 12th December 2019).

8. Saifullah, M. S. M.; Kang, D-J.; Subramanian, K. R. V.; Welland, M. E.; Yamazaki, K.; Kurihara, K. Electron Beam Nanolithography of β-ketoester Modified Aluminium tri-*sec*-butoxide. *J. Sol-Gel Sci. Technol.* **2004**, *29*, 5-10.

9. Subramanian, K. R. V.; Saifullah, M. S. M.; Tapley, E.; Kang, D-J.; Welland, M. E.; Butler, M. Direct Writing of ZrO_2 on a Sub-10 nm Scale using an Electron Beam. *Nanotechnology* **2004**, *15*, 158-162.